Solid State Communications 247 (2016) 68–71

Contents lists available at ScienceDirect

Solid State Communications

journal homepage: www.elsevier.com/locate/ssc

Fast-track communication

Dielectric response of wurtzite gallium nitride in the terahertz frequency range

M.T. Hibberd [a,*], V. Frey [a], B.F. Spencer [a], P.W. Mitchell [a], P. Dawson [a], M.J. Kappers [b], R.A. Oliver [b], C.J. Humphreys [b], D.M. Graham [b]

[a] School of Physics and Astronomy & Photon Science Institute, The University of Manchester, Manchester M13 9PL, United Kingdom
[b] Department of Materials Science and Metallurgy, University of Cambridge, 27 Charles Babbage Road, Cambridge CB3 0FS, United Kingdom

ARTICLE INFO

Article history:
Received 19 July 2016
Accepted 19 August 2016
Available online 21 August 2016

Keywords:
A. Gallium nitride
C. Wurtzite
D. Dielectric constants
E. Terahertz spectroscopy

ABSTRACT

We report on the characterization of the intrinsic, anisotropic, dielectric properties of wurtzite gallium nitride in the spectral range of 0.5–11 THz, using terahertz time-domain spectroscopy. The ordinary ($\tilde{\varepsilon}_{\perp}$) and extraordinary ($\tilde{\varepsilon}_{\parallel}$) components of the complex dielectric function were determined experimentally for a semi-insulating, *m*-plane gallium nitride single crystal, providing measurements of the refractive indices ($n_{\perp,\parallel}$) and absorption coefficients ($\alpha_{\perp,\parallel}$). These material parameters were successfully modeled by considering the contribution of the optical phonon modes, measured using Raman spectroscopy, to the dielectric function, giving values for the relative static dielectric constants of $\varepsilon_{0\perp} = 9.22 \pm 0.02$ and $\varepsilon_{0\parallel} = 10.32 \pm 0.03$ for wurtzite gallium nitride.

1. Introduction

Gallium nitride (GaN) is currently attracting a lot of interest due to its advantages for the development of a wide range of devices operating in the terahertz (THz) frequency regime. Such devices include plasmonic detectors [1,2], quantum cascade lasers [3], and electronic devices operating at THz frequencies, such as resonant tunneling diodes [4]. The development and fundamental understanding of these devices requires knowledge of the relative static dielectric constant of GaN.

The complex dielectric tensor of the most widely used polymorph of GaN, the wurtzite crystal structure, can be fully described by two independent tensor components, $\tilde{\varepsilon}_{\perp}$ and $\tilde{\varepsilon}_{\parallel}$. These two components describe the dielectric dispersion when an electric field is applied either perpendicular or parallel to the [0001] *c*-axis of the crystal. This anisotropic dielectric response of GaN has been well-documented in both the visible [5–7] and mid-infrared [8–11] spectral regions, but there are currently no reported measurements in the literature of the intrinsic dielectric properties at frequencies in the terahertz range.

The mid-infrared dielectric response of wurtzite GaN films have been determined using reflectivity measurements over the range 10–33 μm (from 30 THz down to 9 THz) [10,11]. The static or zero-frequency dielectric constants $\varepsilon_{0\perp,\parallel}$ were also determined from the fitting of the reflectivity spectra. This has led to considerable variation in the literature, with the value of $\varepsilon_{0\perp}$ ranging from 8.9 ± 0.3 [11] to 9.5 ± 0.3 [10] and the value of $\varepsilon_{0\parallel}$ ranging from 9.8 ± 0.3 [11] to 10.4 ± 0.3 [10]. Most recently, Kane et al. [12] used capacitance techniques to measure the real part of $\tilde{\varepsilon}_{\parallel}$ at kHz frequencies and reported a value of 10.6 ± 0.3.

The lower frequencies available from terahertz radiation sources offer the potential for the determination of $\varepsilon_{0\perp,\parallel}$ with greater accuracy than can be determined from mid-infrared measurements. Terahertz time-domain spectroscopy also provides a direct measurement of both the amplitude and phase of transmitted radiation, enabling the determination of the complete complex dielectric function of a material. Despite this, comprehensive studies on GaN are lacking in the terahertz regime. Studies that have been performed report on *c*-plane, *n*-type GaN [13–15] and as a result are restricted to measurements of $\tilde{\varepsilon}_{\perp}$. To measure both $\tilde{\varepsilon}_{\perp}$ and $\tilde{\varepsilon}_{\parallel}$ with a linearly polarized terahertz radiation source at normal incidence requires the *c*-axis to lie in the plane of the material surface, and therefore a non-polar plane of GaN has to be used. Furthermore, while *n*-type material provides useful information about the free-carrier dispersion, the underlying intrinsic dielectric response due to the optical lattice modes is more difficult to determine. Therefore, characterizing a non-polar plane of semi-insulating GaN in the terahertz regime is essential to obtain a complete description of the intrinsic anisotropic dielectric properties for future terahertz device development.

Here we report on the characterization of the dielectric

* Corresponding author.
E-mail address: morgan.hibberd@manchester.ac.uk (M.T. Hibberd).

http://dx.doi.org/10.1016/j.ssc.2016.08.017
0038-1098/

response of a semi-insulating *m*-plane $(1\bar{1}00)$ GaN single crystal in the spectral region from 0.5 to 11 THz, using terahertz time-domain spectroscopy. The $\tilde{\varepsilon}_{\perp}$ and $\tilde{\varepsilon}_{\parallel}$ components of the complex dielectric function were determined over this frequency range. Furthermore, by measuring the optical phonon modes using Raman spectroscopy, we were able to fit the experimental data with the phonon contribution to the dielectric response and obtain values of the relative static dielectric constants.

2. Experimental details

Terahertz transmission measurements were taken with a time-domain spectrometer which used the 50 fs laser pulses provided by an 80 MHz Ti: sapphire oscillator. The generated terahertz radiation was aligned through a 4F confocal geometry of off-axis parabolic mirrors to create focal spots at a sample position and at a detector crystal, and detected using standard electro-optic detection techniques. Two different emitter-detector combinations were used, firstly comprising of an interdigitated gallium arsenide photoconductive antenna (PCA) and a 400 μm-thick (110)-cut gallium phosphide (GaP) detector crystal, and secondly with 100 μm-thick (110)-cut zinc telluride (ZnTe) crystals for generation and detection. The terahertz intensity modulation required for the lock-in amplifier scheme used in balanced electro-optic detection was provided by either modulating the PCA bias or modulating the intensity of the 800 nm generation beam using an acousto-optic modulator. In both cases a modulation frequency of approximately 1 MHz was used to maximize the signal-to-noise ratio of the terahertz waveforms. All measurements were performed at room temperature and in dry air with a relative humidity of less than 10% in order to reduce the absorption of terahertz radiation by water vapor. Two identical stainless steel plates with 3.8 mm diameter apertures were positioned in rotation mounts on a mechanical translation stage at the sample position. The GaN wafer studied was mounted over one aperture allowing alternate reference and sample scans to be taken by translating the stage through the beam path. The wafer holder was rotated by 90° to obtain measurements of the terahertz electric field $\boldsymbol{E}$ aligned both perpendicular and parallel to the *c*-axis of the crystal.

The GaN wafer was a commercially-available (Nanowin Ltd.), semi-insulating *m*-plane $(1\bar{1}00)$ single crystal grown by hydride vapor phase epitaxy. The wafer was 10 mm by 4 mm and had a thickness of 301.8 ± 0.5 μm, as measured with a white-light interferometer (Contour GT-K1, Bruker). The room temperature resistivity of the wafer was reported by the manufacturer to be greater than $10^6\ \Omega$ cm.

Raman spectroscopy was performed at room temperature using a Horiba LabRAM HR Evolution spectrometer with an excitation laser wavelength of 488 nm. Spectra were recorded in a back-scattering geometry with the laser beam incident on either the *c*- or *a*-plane edge faces of the wafer.

3. Results and discussion

The terahertz waveforms obtained for both the PCA-GaP and the ZnTe–ZnTe emitter-detector spectrometer configurations are shown in Fig. 1(a). A time delay offset between the waveforms transmitted through the GaN wafer can be observed between the $\boldsymbol{E}\perp\boldsymbol{c}$ and $\boldsymbol{E}\|\boldsymbol{c}$ orientations, indicating the birefringent nature of non-polar GaN.

For the ZnTe configuration, a multiple reflection of the terahertz pulse within the 100 μm-thick ZnTe crystals can also be seen approximately 2.3 ps after the main pulse. The corresponding power spectra, shown in Fig. 1(b), were calculated from a fast

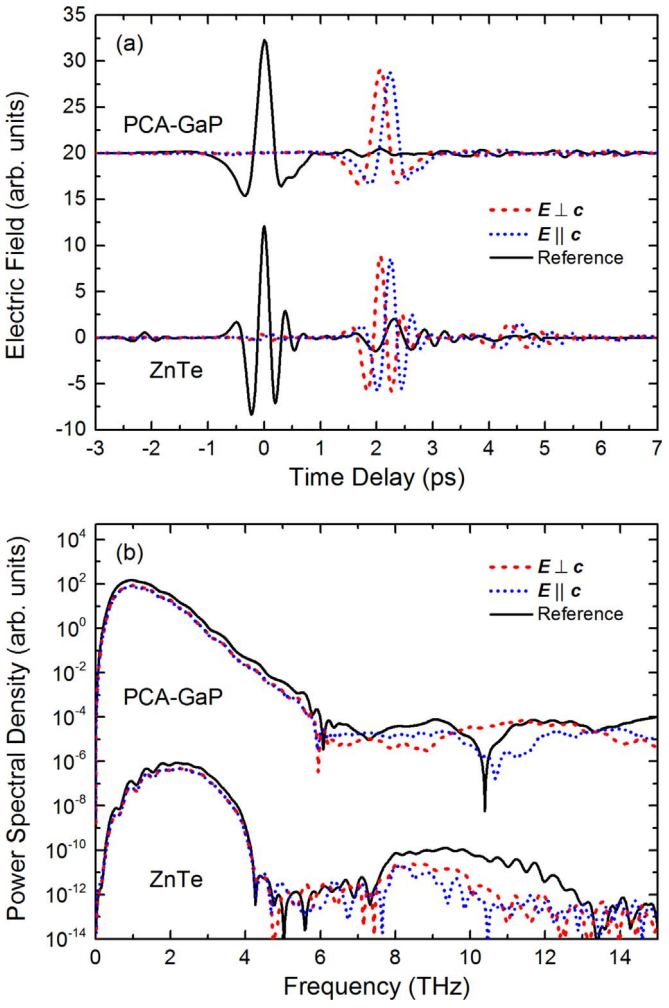

Fig. 1. (a) Terahertz waveforms transmitted through the *m*-plane GaN single crystal using both a PCA-GaP and a ZnTe–ZnTe emitter-detector spectrometer configuration. The waveforms were recorded with the electric field of the terahertz radiation polarized both perpendicular ($\boldsymbol{E}\perp\boldsymbol{c}$) and parallel ($\boldsymbol{E}\|\boldsymbol{c}$) to the *c*-axis of the crystal. (b) The corresponding power spectra. The data for each spectrometer configuration are offset for clarity.

Fourier transform of a 9 ps windowed region of the waveforms that were zero padded to 2^N data points. The windowing was used in order to remove Fourier transform artifacts caused by reflections of the terahertz pulse in the sample while the zero-padding was used to increase the number of data points in the frequency domain. The power spectra demonstrate the different spectral coverage achieved by the two emitter-detector spectrometer configurations. The PCA-GaP setup has continuous coverage up to 5.5 THz, limited primarily by the cancellation of the ionic and electronic contributions to the non-linear susceptibility in GaP around 6–7 THz [16,17]. The ZnTe setup covers a wider frequency range up to approximately 13 THz but the transverse optical (TO) phonon in ZnTe at 5.32 THz [18] results in a loss of the frequency band from 4 to 8 THz. Therefore spectral coverage from 0.5–5.5 THz and 8–11 THz was achieved using the PCA-GaP and ZnTe setups, respectively.

The complex transfer function of the sample, which is the ratio of the transmitted sample, $\tilde{E}(\omega)$, and reference spectra, $\tilde{E}_{\mathrm{ref}}(\omega)$, was determined using [19],

$$\frac{\tilde{E}(\omega)}{\tilde{E}_{\mathrm{ref}}(\omega)} = \frac{4\tilde{n}}{(\tilde{n}+1)^2}\exp\left[-i(\tilde{n}-1)\frac{\omega L}{c}\right]\cdot \mathrm{FP}(\omega), \tag{1}$$

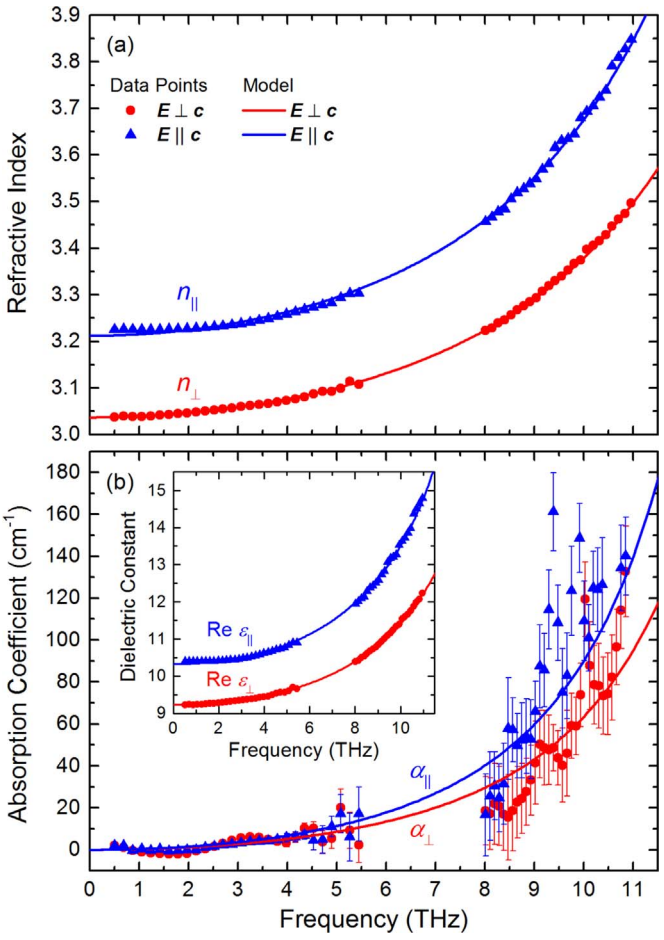

Fig. 2. (a) Refractive index and (b) absorption coefficient values determined from transmission with the terahertz electric field polarized perpendicular ($\boldsymbol{E}\perp\boldsymbol{c}$) and parallel ($\boldsymbol{E}\|\boldsymbol{c}$) to the c-axis of the m-plane GaN single crystal. The data are fitted using a damped harmonic oscillator model of the phonon contribution to the dielectric dispersion given by Eqs. (2) and (3). Inset in (b) shows the real part of the relative dielectric constants.

where $\tilde{n}$ is the complex refractive index of the sample, which is given by $\tilde{n} = n - i\kappa$, where n is the refractive index and κ is the extinction coefficient. L is the sample thickness, ω is the angular frequency of the terahertz radiation, and c is the speed of light. The Fabry-Pérot term, FP(ω), was set equal to 1, since the windowing function was chosen to include only pulses which had made a single pass through the sample.

A fixed-point iteration procedure [19] was used to extract values for n and the absorption coefficient $\alpha = 2\omega\kappa/c$. The results, shown in Fig. 2, were then used to obtain $\tilde{\varepsilon}_{\perp,\|}$ using the well-known relationship $\tilde{\varepsilon}(\omega) = \tilde{n}^2$. For the ZnTe setup, the presence of the TO phonon in ZnTe resulted in a loss of the absolute phase information across the 4–8 THz region, and so a phase correction factor was required to obtain n over 8–11 THz.

Fig. 2(a) shows that the GaN wafer is a positive birefringent crystal because the extraordinary ($n_\|$) refractive index is larger than the ordinary ($n_\perp$) refractive index. The absorption coefficient is plotted in Fig. 2(b) and shows weak absorption with values below 20 cm^{-1} in the 0.5–5.5 THz region. The semi-insulating wafer therefore exhibited excellent transmission, given by $T = (16n^2/(n+1)^4)\exp(-\alpha L)$, with values of 57.0% for $\boldsymbol{E}\perp\boldsymbol{c}$ and 52.2% for $\boldsymbol{E}\|\boldsymbol{c}$ at 1 THz. This is in contrast to the study on unintentionally-doped, n-type ($N = 0.91\times10^{16}\ \mathrm{cm}^{-3}$) GaN [13], which reported a peak in the absorption coefficient at around 0.5 THz of close to 250 cm^{-1}, as a result of the strong absorption of low-frequency terahertz radiation by free carriers.

Zhang et al. [13] used the Drude model, together with a constant value of 9.4 for the real part of $\tilde{\varepsilon}_\perp$, to describe the absorption of their n-type GaN wafers. However, as recognized by the authors of this work [13], their lack of knowledge of the complete complex dielectric response of the intrinsic GaN material resulted in a deviation of their fitting above 2 THz. The semi-insulating wafer employed here allowed the intrinsic properties of GaN to be determined. The measured values for the real part of the dielectric constant, given by $\mathrm{Re}\,\varepsilon = n^2 - (\alpha c/2\omega)^2$, are shown in the inset of Fig. 2(b). Over the measured frequency range, Re ε varies from 9.23 to 12.31 for $\boldsymbol{E}\perp\boldsymbol{c}$, and from 10.40 to 14.83 for $\boldsymbol{E}\|\boldsymbol{c}$. Due to the low value of the absorption coefficient, Re ε is well approximated by n^2. The measured values for the imaginary part of the dielectric constant can be obtained using $\mathrm{Im}\,\varepsilon = n\alpha c/\omega$ together with the values of n and α given in Fig. 2(a) and (b).

For an ionic crystal the intrinsic dielectric response is due to optical phonon modes. According to group-factor analysis [20], there are 6 sets of optical phonon modes in wurtzite GaN, $A_1+E_1+2E_2+2B_1$, from which the polar A_1 and E_1 modes split into longitudinal (LO) and transverse optical (TO) components. The complex dielectric function can therefore be described in terms of the phonon contribution using solutions to Maxwell's equations and treating the phonons as damped Lorentz oscillators. For a uniaxial crystal this also requires both $\tilde{\varepsilon}_\perp$ and $\tilde{\varepsilon}_\|$ components corresponding to $\boldsymbol{E}\perp\boldsymbol{c}$ and $\boldsymbol{E}\|\boldsymbol{c}$ respectively, which are given by [21],

$$\tilde{\varepsilon}_\perp(\omega) = \varepsilon_{\infty\perp} + \frac{(\varepsilon_{0\perp} - \varepsilon_{\infty\perp})\omega_{\mathrm{TO}\perp}^2}{\omega_{\mathrm{TO}\perp}^2 - \omega^2 - i\gamma_{\mathrm{TO}\perp}\omega} \tag{2}$$

and

$$\tilde{\varepsilon}_\|(\omega) = \varepsilon_{\infty\|} + \frac{(\varepsilon_{0\|} - \varepsilon_{\infty\|})\omega_{\mathrm{TO}\|}^2}{\omega_{\mathrm{TO}\|}^2 - \omega^2 - i\gamma_{\mathrm{TO}\|}\omega}, \tag{3}$$

where $\varepsilon_{0\perp,\|}$ and $\varepsilon_{\infty\perp,\|}$ are the static and high frequency dielectric constants, respectively. Since the E_1 phonon vibrates perpendicular to the c-axis, $\omega_{\mathrm{TO}\perp}$ and $\gamma_{\mathrm{TO}\perp}$ correspond to the frequency and damping constant of the E_1(TO) phonon, respectively. Conversely, the A_1 phonon vibrates parallel to the c-axis, so $\omega_{\mathrm{TO}\|}$ and $\gamma_{\mathrm{TO}\|}$ are the equivalent for the A_1(TO) phonon.

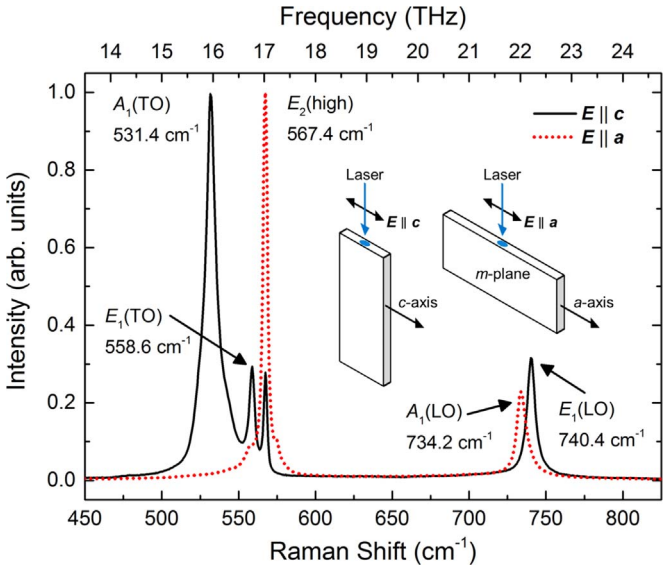

Fig. 3. Raman back-scattering spectra of the m-plane GaN single crystal using edge geometry with the electric field ($\boldsymbol{E}$) polarized parallel to the a- and c-axis, as depicted in the inset.

Table 1
The parameter values used in Eqs. (2) and (3) to model the phonon contribution to the dielectric function.

	$E\perp c$	$E\parallel c$
ε_0	9.22 ± 0.02	10.32 ± 0.03
ε_∞	5.25 ± 0.01	5.41 ± 0.02
$\omega_{TO}/2\pi$ (THz)	16.75 ± 0.01	15.93 ± 0.01
$\omega_{LO}/2\pi$ (THz)	22.20 ± 0.01	22.01 ± 0.01
$\gamma_{TO}/2\pi$ (THz)	0.3 ± 0.1	0.3 ± 0.1

The experimentally measured values of $n_{\perp,\parallel}$ and $\alpha_{\perp,\parallel}$ can be fitted using Eqs. (2) and (3). However, the least-squares fitting procedure employed here is restricted to the $n_{\perp,\parallel}$ data set, due to the lower uncertainties in the measurement of n by THz time-domain spectroscopy [22]. The results of this fitting procedure are shown in Fig. 2(a) and (b) in comparison to both the $n_{\perp,\parallel}$ and $\alpha_{\perp,\parallel}$ data sets. To reduce the number of fitting parameters, Raman scattering measurements were performed to obtain the optical phonon frequencies and damping constant values. The Raman spectra are shown in Fig. 3 using the edge geometry in two back-scattering configurations.

The Raman-active modes that satisfy the selection rules [23] for $\boldsymbol{E}\parallel\boldsymbol{a}$, are the E_2(high) and A_1(LO) modes and for $\boldsymbol{E}\parallel\boldsymbol{c}$, the A_1(TO) and E_1(TO) modes, which can all be observed in Fig. 3. In addition, the forbidden E_1(LO) mode is observed, likely due to either defects or the miscut of the crystal, resulting in breakdown of the selection rules [24]. A Lorentzian line shape fitting was performed to extract the frequency and linewidth of each phonon mode. The values obtained are in excellent agreement with those reported for bulk GaN in the literature [20] and are summarized in Table 1. In addition to using the measured TO phonon frequencies and linewidths, the LO phonon frequency was used together with the Lyddane-Sachs-Teller relationship, $\varepsilon_0/\varepsilon_\infty = (\omega_{LO}/\omega_{TO})^2$, to constrain the ε_0 to ε_∞ ratio. The measured refractive index values were therefore fitted using a single variable fitting parameter, ε_0. The fit was calculated over the useful frequency range, from 0.5 to 5.5 THz and 8 to 11 THz, to determine the values of $\varepsilon_{0\perp,\parallel}$. Table 1 gives $\varepsilon_{0\perp,\parallel}$ and the values of $\varepsilon_{\infty\perp,\parallel}$, which were determined using the phonon frequencies together with the Lyddane-Sachs-Teller relationship.

The values obtained for $\varepsilon_{0\perp,\parallel}$ are lower than the most widely cited values, determined from fitting mid-infrared reflectivity spectra, in the literature [10]. The values are however in excellent agreement with theoretical calculations performed by Wagner et al. [25], who used density-functional perturbation theory to obtain values of 9.24 for $\varepsilon_{0\perp}$ and 10.35 for $\varepsilon_{0\parallel}$. The value obtained for $\varepsilon_{0\parallel}$ is also in good agreement with the 10.28 value determined by Bernardini et al. [26] using a polarization-based calculation of the dielectric tensor of wurtzite GaN.

4. Summary

Terahertz time-domain spectroscopy of a semi-insulating, *m*-plane GaN single crystal enabled both the $\tilde{\varepsilon}_\perp(\omega)$ and $\tilde{\varepsilon}_\parallel(\omega)$ components of the complex dielectric function to be determined, providing a complete description of the intrinsic, anisotropic, dielectric properties of wurtzite GaN at terahertz frequencies. Furthermore, by using Raman spectroscopy to measure the optical phonon modes in the crystal, the dielectric response could be fitted with a damped harmonic oscillator model to determine more accurate values of the static dielectric constants. These results will provide the essential material parameters to assist in the future design of terahertz devices based on wurtzite GaN.

Acknowledgments

This work was supported by the United Kingdom Engineering and Physical Sciences Research Council [Grant numbers EP/J002518/1, EP/J001627/1, and EP/J003603/1]. The authors also wish to thank Suzhou Nanowin Science and Technology Company Ltd. for providing the GaN single crystal used in this study. The data associated with the paper are openly available from The University of Manchester eScholar Data Repository: http://dx.doi.org/10.15127/1.303144.

References

[1] W.D. Hu, L. Wang, X.S. Chen, N. Guo, J.S. Miao, A.Q. Yu, W. Lu, Opt. Quantum Electron. 45 (2013) 713.
[2] K.Y. Xu, Y.N. Wang, C.J. Zheng, J.W. Xiong, G. Wang, J. Nanomater. 2014 (2014) 850915.
[3] C. Ndebeka-Bandou, M. Rösch, K. Ohtani, M. Beck, M.J. Faist, Appl. Phys. Lett. 108 (2016) 091102.
[4] A. Rached, A. Bhouri, S. Sakr, J.-L. Lazzari, H. Belmabrouk, Superlattice Microstruct. 91 (2016) 37.
[5] S. Ghosh, P. Waltereit, O. Brandt, H.T. Grahn, K.H. Ploog, Appl. Phys. Lett. 80 (2002) 413.
[6] S. Shokhovets, R. Goldhahn, G. Gobsch, S. Piekh, R. Lantier, A. Rizzi, V. Lebedev, W. Richter, J. Appl. Phys. 94 (2003) 307.
[7] J. Bhattacharyya, S. Ghosh, B.M. Arora, Appl. Phys. Lett. 91 (2007) 251913.
[8] S.R. Bowman, C.G. Brown, M. Brindza, G. Beadie, J.K. Hite, J.A. Freitas, C.R. Eddy, J.R. Meyer, I. Vurgaftman, Opt. Mater. Express 4 (2014) 1287.
[9] S. Shokhovets, M. Himmerlich, L. Kirste, J.H. Leach, S. Krischok, Appl. Phys. Lett. 107 (2015) 092104.
[10] A.S. Barker, M. Ilegems, Phys. Rev. B 7 (1973) 743.
[11] H. Sobotta, H. Neumann, R. Franzheld, W. Seifert, Phys. Status Solidi B 174 (1992) K57.
[12] M.J. Kane, M.J. Uren, D.J. Wallis, P.J. Wright, D.E.J. Soley, A.J. Simons, T. Martin, Semicond. Sci. Technol. 26 (2011) 085006.
[13] W. Zhang, A.K. Azad, D. Grischkowsky, Appl. Phys. Lett. 82 (2003) 2841.
[14] T.-R. Tsai, S.-J. Chen, C.-F. Chang, S.-H. Hsu, T.-Y. Lin, Opt. Express 14 (2006) 4898.
[15] H.C. Guo, X.H. Zhang, W. Liu, A.M. Yong, S.H. Tang, J. Appl. Phys. 106 (2009) 063104.
[16] J.K. Wahlstrand, R. Merlin, Phys. Rev. B 68 (2003) 054301.
[17] G. Klatt, R. Gebs, C. Janke, T. Dekorsy, A. Bartels, Opt. Express 17 (2009) 22847.
[18] G. Gallot, J. Zhang, R.W. McGowan, T.-I. Jeon, D. Grischkowsky, Appl. Phys. Lett. 74 (1999) 3450.
[19] W. Withayachumnankul, B. Ferguson, T. Rainsford, S.P. Mickan, D. Abbott, Electron. Lett. 41 (2005) 800.
[20] V.Y. Davydov, Y.E. Kitaev, I.N. Goncharuk, A.N. Smirnov, J. Graul, O. Semchinova, D. Uffmann, M.B. Smirnov, A.P. Mirgorodsky, R.A. Evarestov, Phys. Rev. B 58 (1998) 12899.
[21] M. Born, K. Huang, Dynamical Theory of Crystal Lattices, Clarendon Press, Oxford 1954, p. 121.
[22] W. Withayachumnankul, B.M. Fischer, D. Abbott, Terahertz Metrology, Artech House, Boston 2015, pp. 91–114 (Ch. 4).
[23] H. Gao, F. Yan, H. Zhang, J. Li, J. Wang, J. Yan, J. Appl. Phys. 101 (2007) 103533.
[24] G.H. Li, W. Zhang, H.X. Han, Z.P. Wang, S.K. Duan, J. Appl. Phys. 86 (1999) 2051.
[25] J.-M. Wagner, F. Bechstedt, Phys. Rev. B 66 (2002) 115202.
[26] F. Bernardini, V. Fiorentini, D. Vanderbilt, Phys. Rev. Lett. 79 (1997) 3958.